NMR spatial structure of α-conotoxin ImI reveals a common scaffold in snail and snake toxins recognizing neuronal nicotinic acetylcholine receptors

Innokenty V. Maslennikov[a], Zakhar O. Shenkarev[a], Maxim N. Zhmak[a], Vadim T. Ivanov[a], Christoph Methfessel[b], Victor I. Tsetlin[a], Alexander S. Arseniev[a,*]

[a] *Shemyakin-Ovchinnikov Institute of Bioorganic Chemistry, Russian Academy of Science, 16/10 Miklukho-Maklaya, Moscow 117871, Russia*
[b] *Zentrale Forschung, Abteilung Biophysik, Bayer AG, D-51368 Leverkusen, Germany*

Received 4 December 1998

Abstract A 600 MHz NMR study of α-conotoxin ImI from *Conus imperialis*, targeting the α7 neuronal nicotinic acetylcholine receptor (nAChR), is presented. ImI backbone spatial structure is well defined basing on the NOEs, spin-spin coupling constants, and amide protons hydrogen-deuterium exchange data: rmsd of the backbone atom coordinates at the 2–12 region is 0.28 Å in the 20 best structures. The structure is described as a type I β-turn (positions 2–5) followed bya distorted helix (positions 5–11). Similar structural psattern can be found in all neuronal-specific α-conotoxins. Highly mobile side chains of the Asp-5, Arg-7 and Trp-10 residues form a single site for ImI binding to the α7 receptor. When depicted with opposite directions of the polypeptide chains, the ImI helix and the tip of the central loop of long chain snake neurotoxins demonstrate a common scaffold and similar positioning of the functional side chains, both of these structural elements appearing essential for binding to the neuronal nAChRs.

Key words: Nuclear magnetic resonance structure; Neurotoxin; Conotoxin; Acetylcholine receptor

1. Introduction

In recent years α-conotoxins (α-CTx), peptide neurotoxins from the poisonous marine snails of the *Conus* genus, have become very convenient tools for studies on nicotinic acetylcholine receptors (nAChRs), thereby supplementing the arsenal of classical nAChR blockers, the snake venom α-neurotoxins (α-NTx, see reviews [1–4]).

Despite the phylogenetically distant source and considerable differences in size, 12–16 amino acid residues in α-CTx and 60–74 residues in α-NTx, the two families share overlapping binding sites on nAChR, and, moreover, can distinguish different types and subtypes of nAChRs. For example, short chain (60–62 residues) and long chain (66–74 residues) snake α-NTx bind tightly with all muscle-type nAChRs [5], while neuronal nAChRs can be divided into two main groups depending upon their sensitivity or insensitivity to the long chain α-NTx [6]. On the other hand, such members of the α-CTx family as GI, MI, or SI potently inhibit *Torpedo* and muscle (α2βγ(ε)δ) nAChRs [7], while a group of neuronal toxins shows selectivity towards nAChRs built of α7 subunits (ImI), or combinations of different α and β subunits: α3β2 (MII, EpI), α3β4 (EpI) [8–10].

Current methods of molecular biology and peptide chemistry allow researchers to pinpoint the groups essential for toxin-receptor interactions both in receptors and in toxins [11–13]. While the exact mutual disposition of the important residues of the nAChRs is not yet known, this problem can be solved for α-CTx and α-NTx. To date several high resolution X-ray and NMR structures have been determined for α-NTxs (α-bungarotoxin [14], α-cobratoxin [15], neurotoxin I [16], etc.) and α-CTxs (GI [17–19], MI [20], PnIA [21], PnIB [22], MII[23], and EpI [24]).

One of the pharmacologically important nAChRs is the α7 receptor of humans and other mammals. A number of residues in α7 nAChR (Trp-55, Ser-59 and Thr-77) and α-CTx ImI (Asp-5, Arg-7 and Trp-10) essential for toxin-nAChR binding have recently been identified [12,13]. However, the spatial structure of α-conotoxin ImI was not known. One would expect that the spatial structure of ImI could provide new information about the topology of the nAChR binding site and further assist in the interpretation of current data on the specificity of α-CTx and α-NTx for different subtypes of nAChRs.

The present paper describes the elucidation of the three-dimensional structure of α-CTx ImI in aqueous solution with the aid of ^{1}H NMR spectroscopy. The obtained structure is compared with the available X-ray and NMR spatial structures of snail and snake toxins, targeting neuronal nAChRs.

2. Materials and methods

2.1. Synthesis of α-CTx ImI

α-CTx ImI was obtained by chemical synthesis performed on *p*-methylbenzhydryl polymer using Fmoc-Gly, Fmoc-Cys(StBu), Fmoc-Ser(tBu), Fmoc-Asp(OtBu), Fmoc-Pro, Fmoc-Arg(Mtr), Fmoc-Ala, and Fmoc-Trp. Condensations were carried out with the aid of 2-(1*H*-benzotriazol-1-yl)-1,1,3,3-tetramethyluronium tetrafluoroborate. The peptidyl-polymer was first treated for 2 h at 20°C with a TFA:1,2-ethanedithiol:*m*-cresol:dimethyl sulfide (9:03:03:0.3) mixture to remove the protecting groups, and then the peptide was cleaved off from the polymer by HF:*m*-cresol (0°C, 1 h). After evaporating HF, the peptide was precipitated with ether, dried on the filter, and dissolved in 200 ml of 50% aqueous isopropanol. The solution was adjusted to pH 8–9 with diisopropylethylamine, and oxidized on the air (20°C, 18 h). After lowering the pH to 5.0 with acetic acid, the solution was partially evaporated, diluted with water and lyophilized. ImI was isolated on a Nucleosil C18 column using a

*Corresponding author. Fax: (7) (095) 335-50-33.
E-mail: aars@nmr.ru

Abbreviations: α-CTx, α-conotoxin; α-NTx, α-neurotoxin; nAChR, nicotinic acetylcholine receptor; NOE, nuclear Overhauser enhancement; NOESY, 2D NOE-correlated spectroscopy; TOCSY, 2D total correlated spectroscopy

Coordinates of α-conotoxin ImI have been deposited in the Brookhaven Protein Data Bank under accession code 1IMI.

PII: S0014-5793(99)00069-1

Table 1
Analysis of the 20 best structures of α-conotoxin ImI

Parameter	Quantity	Unit	DYANA
Target function	average ± S.D.	Å^2	0.15 ± 0.06
Number of distance constraints upper/lower	NOE		108/119
	disulfide bridge		6/6
	hydrogen bond		6/6
Number of torsion angle constraints	backbone		6
	side chain		6
Upper constraint violations	sum ± S.D.	Å	0.74 ± 0.35
	maximum	Å	0.16
Lower constraint violations	sum ± S.D.	Å	0.24 ± 0.07
	maximum	Å	0.06
van der Waals constraint violations	sum ± S.D.	Å	0.20 ± 0.04
	maximum	Å	0.03
Angle constraint violations	sum ± S.D.	degrees	2.2 ± 0.3
	maximum	degrees	0.8
R^x factor			0.056
rmsd of atom coordinates for 2–12 region	backbone	Å	0.28 ± 0.12
	all heavy atoms	Å	1.74 ± 0.39

linear gradient of acetonitrile in 0.1% aqueous TFA. The yield was 25% (calculated for the starting cysteine). The ImI structure was confirmed by electrospray mass spectrometry (M 1350.48 (calc.), M 1350.71 (found)) and NMR spectroscopy.

2.2. Biological activity of synthetic ImI

The biological activity of synthetic ImI was tested on *Xenopus* oocytes injected with cDNA encoding rat brain α7 nAChR. A two-electrode voltage clamp was used. The extracellular solution, frog Ringer, was perfused at 5 ml/min, whereas perfusion was turned off during incubation of the cells with ImI. Simultaneous application of acetylcholine (50 μM) and ImI (5 μM) resulted in almost complete block of the current. Therefore, our synthetic ImI is equipotent to the toxin used in [25].

2.3. NMR spectroscopy and data processing

6 mg of ImI was dissolved in 600 μl of H_2O (10% D_2O) or D_2O (100% deuterium, SIL, UK). ^{1}H NMR spectra were obtained at pH 5.5 and 5°C using a 600 MHz (Varian Unity 600) spectrometer. This temperature proved optimal for obtaining NOEs in ImI. DQF-COSY [26], TOCSY [27] with mixing times (τ_m) of 40 and 80 ms, and NOESY [28] with τ_ms of 100, 200 and 400 ms were recorded in the pure phase-absorption mode by collecting hypercomplex data [29]. The WATERGATE [30] and FLIP-BACK [31] techniques were used for the suppression of HOH resonance. A relaxation delay of 2.0 s was used. Chemical shifts were measured relative to the HOH signal, the chemical shift of the latter being arbitrarily chosen as 5.0 ppm at 5°C relative to tetramethylsilane. Proton spin-spin coupling constants (10 H-NC$^\alpha$-H and 16 H-C$^\alpha$C$^\beta$-H) were measured in 1D spectra with a digital resolution of 0.5 Hz/point.

To detect amide protons with slow hydrogen-deuterium exchange rates, 1D spectra were recorded starting at 10, 20 and 40 min on ImI solution in D_2O, pH 5.5, 5°C.

NMR spectra were processed with VNMR, Varian software. Complete proton resonance assignment was performed by a standard procedure [32] using the XEASY program [33]. Cross-peak intensities in NOESY spectra were measured using an algorithm of non-linear least squares approximation for lineshapes of cross-peak sections in both directions of 2D spectra implemented in the XEASY program.

2.4. Experimental constraints

Interproton distance constraints were derived from the cross-peak intensities measured in NOESY spectra acquired with $\tau_m = 200$ ms where spin-diffusion effects might be ignored. 139 meaningful interproton distance constraints were derived from 286 unambiguously assigned NOESY cross-peak volumes via '$1/r^6$' calibration using the CALIBA program [34]. Refined 108 upper and 119 lower constraints were derived by the complete relaxation matrix approach (program MARDIGRAS [35]) at the final stages of structure calculation. The rotational correlation time was estimated to be 1.0 ns in relaxation matrix calculations according to the size of ImI and water viscosity at 5°C. An additional six upper and six lower distance constraints were introduced for two disulfide bonds between residues Cys-2–Cys-8 and Cys-3–Cys-12. Stereospecific assignments of methylene protons were obtained for six residues with the use of the GLOMSA program [34] based on combination of the available spin-spin coupling constants and NOE-derived distance constraints. Pseudoatom constraints were utilized in cases when the stereospecific assignment for prochiral centers was unknown. Twelve torsion angle constraints were derived from spin-spin coupling constants of H-NC$^\alpha$-H (φ angle) and H-C$^\alpha$C$^\beta$-H (χ^1 angle) protons, and the stereospecific assignments, obtained as described above.

2.5. Spatial structure calculation

Spatial structure calculation was performed using the DYANA program [36]. After generation of the set of 50 structures conforming to '$1/r^6$'-calibrated interproton upper distance and torsion angle constraints, six additional lower distance constraints (3.0 Å) based on cross-peaks expected according to the structures obtained but not present in NOESY spectra were introduced. The value of 3.0 Å is quite cautious, as the smallest of the observed NOEs corresponds to 5.6 Å upper distance constraint. Upper (NH...O 2.3 Å, N...O 3.3 Å) and lower (NH...O 1.8 Å, N...O 2.8 Å) distance constraints were introduced for hydrogen bonds detected in more than 30 out of the 50 calculated structures and confirmed by slow hydrogen-deuterium exchange rates of corresponding amide protons. The next generation of 50 structures was calculated with addition of hydrogen bonds and lower distance constraints and was used for the refinement of the upper distance constraints and generation of lower distance constraints in the MARDIGRAS program. In the last round of calculations, the 20 best structures out of 100 started with the refined distance constraints were selected accounting to the following criteria:

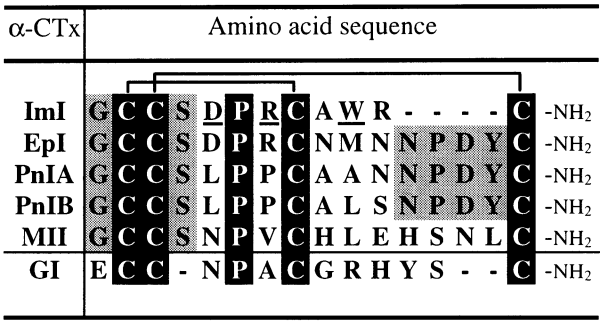

Fig. 1. Amino acid sequences for the five neuronal-selective (top) and one muscle-selective (bottom) α-conotoxins. The conserved proline and cysteine frameworks are shown in black and other residues conserved in neuronal α-conotoxins are shown in gray. The residues essential for ImI interaction with α_7 nAChR [Sine] are underlined. The disulfide bridges are shown at the top of the sequences.

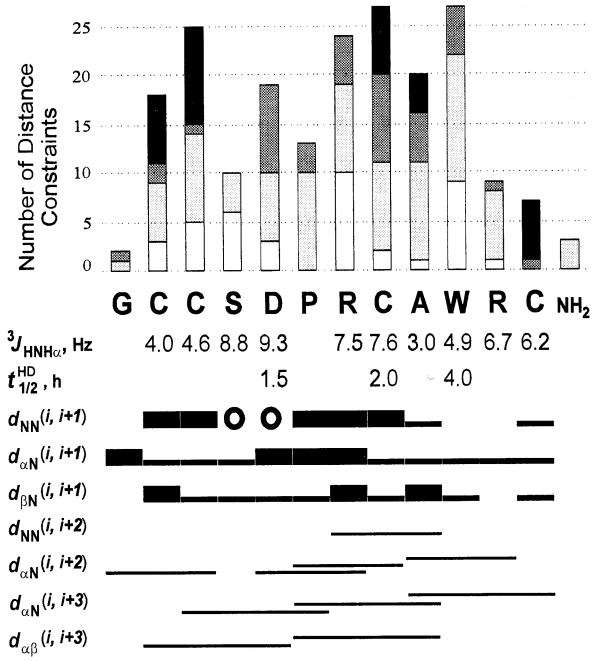

Fig. 2. Overview of NMR data collected for ImI at pH 5.5 and 5°C. NOE connectivities are designated as usual: $d_{AB}(i,j)$ is the connectivity between the proton types A and B located in the amino acid residues i and j, respectively, where N, α and β denote the amide, H^{α} and H^{β} protons. Full-size squares denote a high intensity, half squares a medium, and lines a low intensity of corresponding cross-peaks in the NOESY 200 ms spectrum. The circle indicates overlapping cross-peaks. Values of $^{3}J_{HN-C^{\alpha}H}$ coupling constants and half-exchange times of amide protons ($t_{1/2}^{HD}$) demonstrating slow exchange with solvent deuterons are shown in corresponding lines. The number of distance constraints, used in structure calculation, is shown at the top of the figure. White, light gray, dark gray and black rectangles correspond to intraresidue, sequential ($|i-j|\leq 1$), medium-range ($|i-j|\leq 4$) and long-range ($|i-j|>4$) constraints, respectively.

(i) each structure differs from all others by rmsd of backbone atom coordinates ≥ 0.05 Å and (ii) low final DYANA target function ≤ 0.3 Å^2.

The R^x factor for assessing the conformity of the experimental and theoretical NOE intensities was calculated as in [35]. Visual analysis of the structures obtained and preparation of the figures were performed using the MOLMOL program [37].

3. Results and discussion

The complete resonance assignment for ImI from *Conus imperialis* snail venom was obtained using standard procedures on the basis of DQF-COSY, TOCSY ($\tau_m = 40$ and 80 ms) and NOESY ($\tau_m = 200$ and 400 ms) spectra. A single set of signals in the NMR spectra testifies to the absence of impurities, disulfide isomers, or *cis-trans* Asp-5–Pro-6 peptide bond isomers in the ImI sample. The *trans* orientation of the Asp-5–Pro-6 peptide bond was established based on the intensive cross-peaks between the $C^{\alpha}H$ proton of Asp-5 and $C^{\delta}H_2$ protons of Pro-6.

A summary of the NMR data used in spatial structure calculation is shown in Fig. 2.

The spatial structure was calculated on the assumption that a single ImI backbone conformation is consistent with all available experimental data. The correctness of this assumption is confirmed by: (i) small constraint violations, (ii) low R^x factor value, (iii) small average pairwise rmsd (see Table 1), and (iv) scatter plot of φ and ψ torsion angles (Fig. 3) in the obtained set of structures.

The ImI spatial structure is shown in Fig. 4. Residues Cys-2–Asp-5 and Arg-7–Trp-10 form type I β-turns, connected by a half-turn Ser-4–Arg-7. The region from Asp-5 to Arg-11 can be considered a short distorted helix (Fig. 4). The N-terminal Gly-1 possesses a high conformational mobility, confirmed by degenerated chemical shifts of its $C^{\alpha}H$ protons. Relatively low intensities of sequential NOE cross-peaks and the averaged values of $^{3}J_{HN-C^{\alpha}H} \approx 6.5$ Hz of Arg-11–Cys-12 (Fig. 2) testify that their backbone is less ordered than the Cys-2–Trp-10 region. The slowly exchanging amide protons (Fig. 2) form three hydrogen bonds NH(Asp-5)–CO(Cys-2), NH(Cys-8)–CO(Asp-5) and NH(Trp-10)–CO(Pro-6) which stabilize the spatial structure of ImI.

The Arg-7 residue displaying small (4.0 Hz) and large (10.6 Hz) $^{3}J_{HC^{\alpha}-C^{\beta}H}$ has one most populated ($80 \pm 10\%$) χ^1 rotamer ($180 \pm 30°$). The small $^{3}J_{HC^{\alpha}-C^{\beta}H}$ values (3.0 and 5.0 Hz) of Ser-4 correspond to two χ^1 rotamers of $+60 \pm 30°$ (population $80 \pm 10\%$) and $180 \pm 30°$ ($20 \pm 10\%$). The averaged $^{3}J_{HC^{\alpha}-C^{\beta}H}$ values of Asp-5 and Trp-10 and the degenerated chemical shifts of Arg-11 $C^{\beta}H_2$, $C^{\gamma}H_2$ and $C^{\delta}H_2$ protons are indicative of a free rotation of the corresponding side chains. All four cysteine residues (2, 3, 8 and 12) have small (~ 4.1 Hz) and large (> 10.0 Hz) $^{3}J_{HC^{\alpha}-C^{\beta}H}$ values, which correspond to $\chi^1 = 180 \pm 30°$. The Cys-2–Cys-8 disulfide bridge has a left-handed configuration ($\chi^3 = -113° \pm 6°$), while the Cys-3–Cys-12 disulfide bridge has a right-handed one ($\chi^3 = 98 \pm 19°$). The conservative proline residue (position 5 in GI and 6 in neuronal α-CTx, Fig. 1) determines the conformation of the X-Pro-X region, which is similar (half-turn or 90° turn) in all α-CTx with known spatial structures. The significant structural role of Pro-6 is evident from the loss of activity in proline-substi-

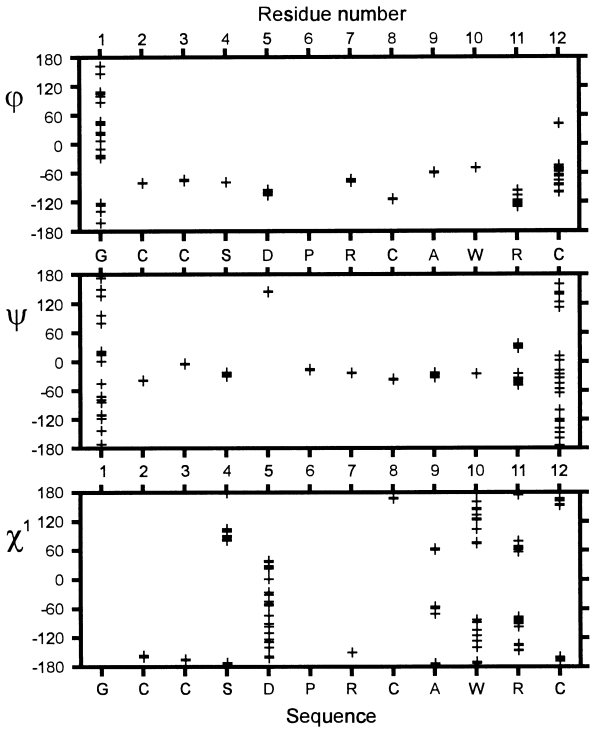

Fig. 3. Scatter plot of the φ, ψ, χ^1 angles for the 20 best DYANA structures of ImI. The sequence of ImI is shown at the bottom.

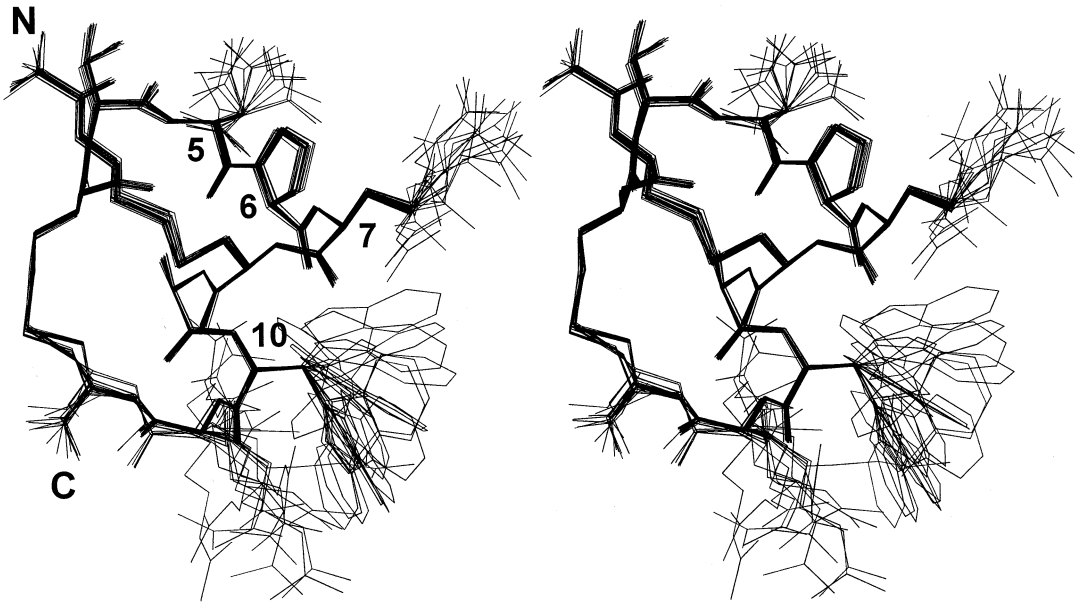

Fig. 4. Stereoview of the 20 best structures of ImI, superimposed on the backbone atoms of the 2–12 region. The residues essential for ImI structure and function are numbered.

tuted MI [38] and ImI [13] analogues. Thus, the backbone structure of ImI is constrained by the two disulfide bridges and proline conservative for all α-CTxs, which force the backbone to form continuous turns.

The critical Asp-5, Pro-6, Arg-7 and Trp-10 residues, providing ImI specificity for the α7 nAChR [13], are clustered at one site of the ImI spatial structure (Fig. 4). Interestingly, three of the four critical residues have highly mobile side chains (Figs. 3 and 4). On the other hand, essential residues in the muscle-specific α-CTx GI have fixed side chains but are located at the flexible region of the backbone [18]. Hence, one would expect that certain conformations of the critical side chains (for ImI) or the backbone (for GI) are selected upon binding with the respective receptor. Even though upon such binding the conformational entropy of the ligand decreases, the loss could be compensated by a good fit of the complementary surfaces of the ligand and the receptor and by the removal of immobilized water from the surfaces.

The high-resolution spatial structures of five neuronal-specific α-CTx (PnIA [21], PnIB [22], MII [23], [Tyr^{15}]EpI [24] and ImI [present work]) and two muscle-specific α-CTx, GI [17–19] and MI [20], are known. The size of ImI (12 residues) is closer to the muscle-specific α-CTxs GI and MI (13 and 14 residues, respectively) than to the neuronal-specific α-CTxs PnIA, PnIB, MII and EpI (all have 16 residues). However, the difference in the cysteine framework (3/5-type for GI and MI versus 4/3-type for ImI, Fig. 1) does not allow ImI to form the GI-like 'flat triangle' structure [17]. Surprisingly, the scaffold of all four 16 residues long neuronal α-CTx (PnIA [21], PnIB[22], MII [23] and [Tyr^{15}]EpI [24]) displays a remarkable

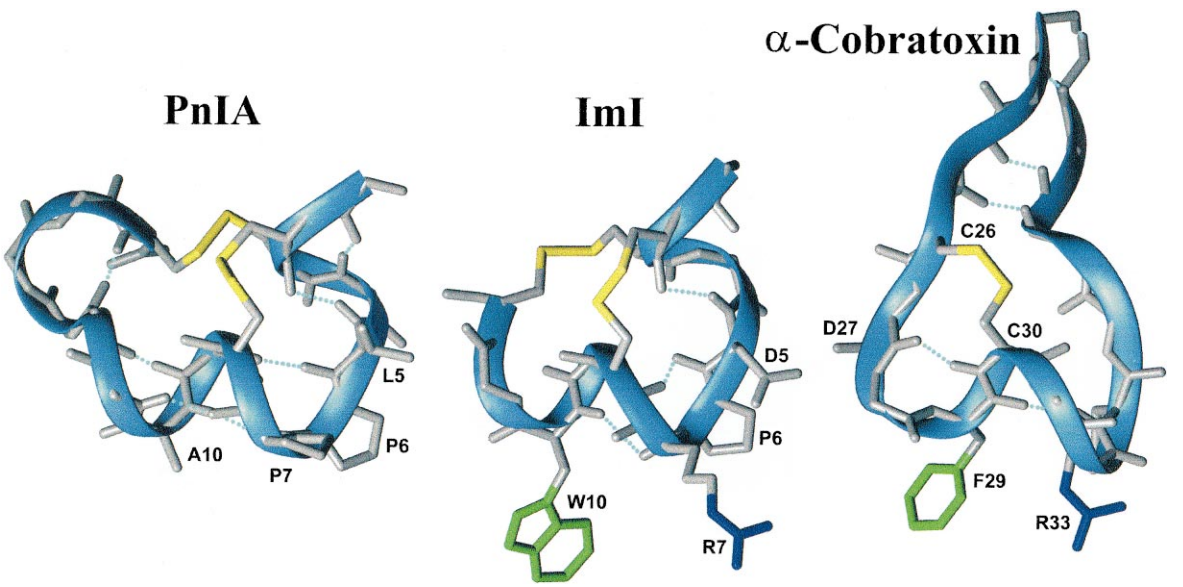

Fig. 5. Ribbon representation of the spatial structures of neuronal-specific α-conotoxins PnIA [21] and ImI (present work) and the central loop region (residues 24–37) of α-cobratoxin [15]. Hydrogen bonds are shown in dotted lines. Side chains of the essential residues are shown.

similarity to that of ImI (Fig. 5) despite different cysteine frameworks (Fig. 1).

While the scaffold of the ImI 'active site' determined by cysteine and proline residues is conservative, the functionally essential side chains (positions 5, 7 and 10) of ImI demonstrate high variability within the neuronal-specific α-CTx family (Fig. 1). The variability of the critical side chains provides distinct selectivities of α-CTx for different neuronal nAChR subtypes. At the same time, Gly-1 and Ser-4 are two of the conservative residues in neuronal-specific α-CTx (Fig. 1), but both are situated outside the ImI active site (Fig. 4) and are not strictly necessary for ImI binding with α7 nAChR [13].

Interestingly, the helical scaffold and the disposition of aromatic and guanidinium groups in the ImI active site are very similar to those of the central loop tip in all long chain α-NTxs (Fig. 5): α-bungarotoxin [14], α-cobratoxin *Naja naja siamensis* [15], neurotoxin I *Naja naja oxiana* [16], and κ-bungarotoxin [39]. The central loop tip of the long chain snake α-NTxs forms a helical-like structure consisting of the two sequential turns and maintained by a disulfide bridge (Cys-26–Cys-30 in α-cobratoxin), which is present in the long but not in the short chain α-NTxs. The latter have a quite different conformation of the central loop tip. The structural similarity between the neuronal α-CTx and the tip of the long chain α-NTx central loop is most pronounced when their polypeptide chains are depicted in opposite directions (Fig. 5). The 'reversed homology' in the amino acid sequences of α-CTx GI and the central loop tip of the short chain α-NTx (both specific for muscle receptors) was observed earlier [40].

The fact that ImI and GI mimic one of the binding sites of the long chain and short chain α-NTxs, respectively, may shed light on the structural basis of distinct selectivities of different groups of snail and snake toxins towards muscle- and/or neuronal-type nAChRs. Indeed, the short chain and long chain α-NTxs have comparable affinities for muscle-type nAChRs [5]. On the other hand, the high affinity (in the nanomolar range) for neuronal α7 nAChR receptors is inherent only in long chain α-NTxs, whereas for short α-NTxs the K_d values are at best in the micromolar range [41]. Removal of the fifth disulfide bridge by reduction in α-cobratoxin [41], or Ala substitution of the respective cysteines in κ-bungarotoxin [11], diminishes the toxins' affinity for the α7 and α3/β2 neuronal receptors, respectively, to that of short α-NTx. Clearly, the central loop disulfide bridge of long chain α-NTx maintains the ImI-like helical scaffold, which in turn determines the appropriate disposition of the essential side chains (Fig. 5).

As shown in [13] AspProArg and Trp residues are strictly essential for ImI binding to the α7 receptor. In other words, the combination of carboxylate, a guanidinium group and an aromatic ring, arranged in a certain geometry on the ImI helical scaffold, provides a quite efficient ($K_d \approx 10^{-7}$ M) interaction with the α7 receptor [13]. Similar groups are found in the central loop of long and short chain α-NTxs, but apparently due to differences in the scaffold of the central loops their spatial dispositions vary, which in turn underlies the observed distinct specificities for various types of nAChRs. Thus, the helical scaffold of the central loop is one of the structural determinants required for high affinity binding of the long chain α-NTxs to neuronal nAChRs. Apparently, the interactions of loops I and III of long chain α-NTxs, which are known to be important for binding to muscle-type nAChR, also contribute to binding to neuronal receptors. That is why disruption of the helical scaffold diminishes binding of the long chain α-NTxs to α7 and α3β2 neuronal nAChRs, but does not abolish it completely [11,41].

α Subunits of the muscle- and neuronal-type nAChRs were suggested to have a common scaffold [12] and α-helices were hypothesized to be present in the ligand binding sites of the *Torpedo* α subunits [42,43]. Interestingly, two of the three (Trp-55, Ser-59 and Thr-77) residues of the α7 subunit critical for ImI binding [12] have the *i*,*i*+4 periodicity typical of α-helices. In the light of these data we can speculate that the helical scaffold found in neuronal-specific α-CTx and in long chain α-NTxs is important for recognizing a helical motif in the ligand binding site of nAChRs.

Acknowledgements: This work was partly supported by RFBR Grants to I.V.M. (98-04-48685) and V.I.T. (96-04-50375) and by a grant from Bayer AG (Leverkusen, Germany).

References

[1] Changeux, J.-P. and Lena, C. (1998) J. Physiol. (Paris) 92, 63–74.
[2] Hucho, F., Tsetlin, V.I. and Machold, J. (1996) Eur. J. Biochem. 239, 539–557.
[3] Endo, T. and Tamiya, N. (1991) in: Snake Toxins (Harvey, A.L., Ed.), pp. 165–222, Pergamon Press, New York.
[4] Olivera, B.M. (1997) Mol. Biol. Cell 8, 2101–2109.
[5] Albuquerque, E.X., Eldefrawi, A.T. and Eldefrawi, M.E. (1979) Handb. Exp. Pharmacol. 52, 377–402.
[6] Clarke, P.B.S. (1992) Trends Pharmacol. Sci. 13, 407–413.
[7] Myers, R.A., Cruz, L.J., Rivier, J.E. and Olivera, B.M. (1993) Chem. Rev. 93, 1923–1936.
[8] McIntosh, J.M., Yoshikami, D., Mahe, E., Nielsen, D.B., Rivier, J.E., Gray, W.R. and Olivera, B.M. (1994) J. Biol. Chem. 269, 16733–16739.
[9] Cartier, G.E., Yoshikami, D., Gray, W.R., Luo, S., Olivera, B.M. and McIntosh, J.M. (1996) J. Biol. Chem. 271, 7522–7528.
[10] Loughnan, M., Bond, T., Atkins, A., Jones, A., Gehrmann, J., Cuevas, J., Adams, D.J., Broxton, N., Livett, B., Down, J., Alewood, P.F. and Lewis, R.J. (1998) J. Biol. Chem. 273, 15667–15674.
[11] Grant, G.A., Luetje, C.W., Summers, R. and Xu, X.L. (1998) Biochemistry 37, 12166–12171.
[12] Quiram, P.A. and Sine, S.M. (1998) J. Biol. Chem. 273, 11001–11006.
[13] Quiram, P.A. and Sine, S.M. (1998) J. Biol. Chem. 273, 11007–11011.
[14] Love, R.A. and Stroud, R.M. (1986) Protein Eng. 1, 37–46.
[15] Betzel, C., Lange, G., Pal, G.P., Wilson, K.S., Maelicke, A. and Saenger, W. (1991) J. Biol. Chem. 266, 21530–21536.
[16] Nickitenko, A.V., Michailov, A.M., Betzel, C. and Wilson, K.S. (1993) FEBS Lett. 320, 111–117.
[17] Guddat, L.W., Martin, J.A., Shan, L., Edmundson, A.B. and Gray, W.R. (1996) Biochemistry 35, 11329–11335.
[18] Maslennikov, I.V., Sobol, A.G., Gladky, K.V., Lugovskoy, A.A., Ostrovsky, A.G., Tsetlin, V.I., Ivanov, V.T. and Arseniev, A.S. (1998) Eur. J. Biochem. 254, 238–247.
[19] Gehrmann, J., Alewood, P.F. and Craik, D.J. (1998) J. Mol. Biol. 278, 401–415.
[20] Gouda, H., Yamazaki, K., Hasegawa, J., Kobayashi, Y., Nishiuchi, Y., Sakakibara, S. and Hirono, S. (1997) Biochim. Biophys. Acta 1343, 327–334.
[21] Hu, S.-H., Gehrmann, J., Guddat, L.W., Alewood, P.F., Craik, D.J. and Martin, J.L. (1996) Structure 4, 417–423.
[22] Hu, S.-H., Gehrmann, J., Alewood, P.F., Craik, D.J. and Martin, J.L. (1997) Biochemistry 36, 11323–11330.
[23] Shon, K.-J., Koerber, S.C., Rivier, J.E., Olivera, B.M. and McIntosh, J.M. (1997) Biochemistry 36, 15693–15700.
[24] Hu, S.-H., Loughnan, M., Miller, R., Weeks, C.M., Blessing, R.H., Alewood, P.F., Lewis, R.J. and Martin, J.L. (1998) Biochemistry 37, 11425–11433.
[25] Johnson, D.S., Martinez, J., Elgoyhen, A.B., Heinemann, S.F. and MsIntosh, J.M. (1995) Mol. Pharmacol. 48, 194–199.

[26] Rance, M., Sorensen, O.W., Bodenhausen, G., Wagner, C., Ernst, R.R. and Wuthrich, K. (1983) Biochem. Biophys. Res. Commun. 117, 479–485.
[27] Bax, A. and Davis, D.G. (1985) J. Magn. Reson. 65, 355–366.
[28] Jeener, J., Meier, G.H., Bachman, P. and Ernst, R.R. (1979) J. Chem. Phys. 71, 4546–4553.
[29] States, D.J., Habercorn, R.A. and Ruben, D.J. (1982) J. Magn. Reson. 48, 286–292.
[30] Piotto, M., Saudek, V. and Sklenar, V. (1992) J. Biomol. NMR 2, 661–665.
[31] Lippens, G., Dhalluin, C. and Wieruszeski, J.-M. (1995) J. Biomol. NMR 5, 327–331.
[32] Wuthrich, K. (1986) NMR of Proteins and Nucleic Acids, John Wiley and Sons, New York.
[33] Bartels, C., Xia, T.-h., Billeter, M., Guntert, P. and Wuthrich, K. (1995) J. Biomol. NMR 6, 1–10.
[34] Guntert, P., Braun, W. and Wuthrich, K. (1991) J. Mol. Biol. 217, 517–530.
[35] Borgias, B.A. and James, T.L. (1990) J. Magn. Reson. 87, 475–487.
[36] Guntert, P., Mumenthaler, C. and Wuthrich, K. (1997) J. Mol. Biol. 273, 283–298.
[37] Koradi, R., Billeter, M. and Wuthrich, K. (1996) J. Mol. Graphics 14, 51–55.
[38] Hashimoto, K., Uchida, S., Yoshida, H., Nishiuchi, Y., Sakakibara, S. and Yukari, K. (1985) Eur. J. Pharmacol. 118, 351–354.
[39] Dewan, J.C., Grant, G.A. and Sacchettini, J.C. (1994) Biochemistry 33, 13147–13154.
[40] Gray, W.R., Middlemas, D.M., Zeikus, R., Olivera, B.M. and Cruz, L.J. (1985) in: Peptides, Structure and Function. Proceedings of the 9th American Peptide Symposium (Deber, C.M., Hruby, V.J. and Kopple, S., Eds.), Pierce Chemical Co., Rockford, IL.
[41] Servent, D., Winckler-Dietrich, V., Hu, H.-Y., Kessler, P., Drevet, P., Bertrand, D. and Menez, A. (1997) J. Biol. Chem. 272, 24279–24286.
[42] Tsygelny, I., Sugiyama, N., Sine, S.M. and Taylor, P. (1997) Biophys. J. 73, 52–66.
[43] Unwin, N. (1996) J. Mol. Biol. 257, 586–596.